

# Seabed Characterization Using Acoustic Communication Signals on an Autonomous Underwater Vehicle With a Thin-Line Towed Array

Nicholas P. Chotiros, *Member, IEEE*, and Venugopalan Pallayil, *Senior Member, IEEE*

**Abstract**—Sediment classification was demonstrated using the self-noise of an autonomous underwater vehicle (AUV) received on a short towed array. The adopted approach was to separate the direct path and the surface- and bottom-reflected signals. Electrical interference from the source was used to verify source receiver separation. The amplitude ratio of the bottom reflected to the direct path signal levels, after compensating for the differences in absorption, spreading losses, and beam patterns, yields the bottom-reflection loss, at the applicable grazing angle. The latter is calculated from the travel time difference between the direct path and bottom-reflected signals. The method is self-calibrating, requiring absolute calibration of neither sound source nor receivers. The definitive isolation of the reflected and direct path signals and the self-calibrating property make this approach robust. The reflection loss may be compared to known seabed models to estimate sediment type.

**Index Terms**—Marine sediment, reflection loss, towed array, underwater acoustics.

## I. INTRODUCTION

THE inversion of seabed properties from the reflected acoustic wave, using a known source and a horizontal line array or streamer, towed by a research or survey ship, is a standard procedure [1]–[3]. Sound is projected at the seabed and the reflected signals are received by the line array and processed to measure the reflected signal, which is then used to invert for the properties and layering within the seabed. Recently, the source and receiving array have been miniaturized and deployed on an autonomous underwater vehicle (AUV) [4]–[6]. Instead of a dedicated sound source, sources of opportunity, such as the self-noise of the tow ship, have been used in conjunction with a matched-field technique to achieve a model-based inversion of the sediment strata [7]. In this paper,

a robust measurement of the seabed-reflection loss, using the self-noise of an AUV, towing a thin-line horizontal array, is demonstrated.

The approach adopted was to separate the direct path and the surface- and bottom-reflected signals. The amplitude ratio of the bottom reflected to the direct path signal levels, after compensating for the differences in absorption, spreading losses, and beam patterns, yields the bottom-reflection loss, at the applicable grazing angle. The latter is calculated from the travel time between the source and the receiver and the height above bottom. The method is self-calibrating and requires absolute calibration of neither the sound source nor receivers. The definitive isolation of the reflected and direct path signals, and the self-calibrating property, make this approach robust.

The concept is illustrated in Fig. 1. The bottom, source, and receiver depths are represented by  $d_b$ ,  $d_s$ , and  $d_i$ , where  $i$  is the receiver number with values from 0 to 10. The horizontal distance from the source to the first receiver is  $x_o$  and the horizontal separation between adjacent receivers is  $x_d$ .

Trials were conducted off a pier near the NATO Undersea Research Centre (NURC) office in La Spezia, Italy. The main objectives were to evaluate the performance of the digital thin line array (DTLA) [8], [9] in terms of the signal quality received and its beamforming capability. Seabed-type characterization was not part of the initial plan, but was added at the postprocessing stage. The experiments were performed from June 19 to 23, 2009. The tow platform used was the Ocean Explorer (OEX), an AUV developed at NURC. The DTLA was developed by the Acoustics Research Laboratory, National University of Singapore, Singapore. It was 10.5 m in diameter and about 20 m long with its tow cable included. The data used for this study were from recordings collected on June 23, 2009. The AUV was making rectangular loops of  $250 \times 50 \text{ m}^2$  and the total data collection was for 40 min over four such loops. The speed of tow during these experiments varied from 1.4 to 2.8 kn. The experiment took place in the inner part (within the breakwater) of the Gulf of La Spezia, near the NATO Undersea Research Centre. The sea surface was calm.

The initial intention was to use the self-noise generated by the propulsion system, but it was undetectable above the ambient noise at the test site. However, the acoustic communications (AC) signal was very clearly detected and was put to use. There were a few complications which made the project challenging and unique. 1) There were no separate recordings of the transmitted AC signal. Therefore, the signal was treated as a random noise and only its statistical properties, particularly

Manuscript received January 17, 2012; revised July 16, 2012; accepted October 30, 2012. Date of publication January 08, 2013; date of current version July 10, 2013. This work was supported in part by the U.S. Office of Naval Research under Grants N00014-06-1-0125 and N000141210168.

**Associate Editor:** G. Potty.

N. P. Chotiros is with the Applied Research Laboratories, The University of Texas at Austin, Austin, TX 78713-8029 USA (e-mail: chotiros@arlut.utexas.edu).

V. Pallayil is with the Acoustic Research Laboratory, Tropical Marine Science Institute, National University of Singapore, Singapore 119223, Singapore (e-mail: venu@arl.nus.edu.sg).

Color versions of one or more of the figures in this paper are available online at <http://ieeexplore.ieee.org>.

Digital Object Identifier 10.1109/JOE.2012.2227546

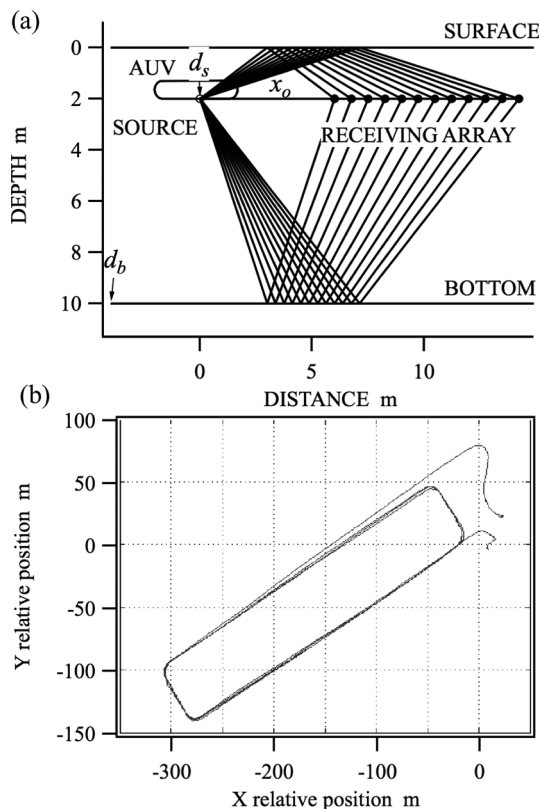


Fig. 1. (a) Concept of the bottom and surface-reflection simulation model, showing a source on an AUV and a towed receiving array, and single-bounce bottom- and surface-reflected rays. (b) Plan view of AUV track loops. The origin of the coordinate system is approximately  $44^{\circ}5'41''$  N and  $9^{\circ}51'43''$  E.

the autocorrelation and cross-correlation functions, could be relied upon. 2) There was a strong electrical feed-over from the AC acoustic projector into the receiving amplifiers, but instead of being a hindrance, it was useful for estimating the separation between the source and the receivers. 3) The autocorrelation function of the AC signal had undesirable time sidelobes. 4) The sediment at the test site was very soft, and, consequently, the reflected signal was weak, and it was necessary to coherently stack the correlation functions to find the bottom echo.

The paper is arranged as follows. Section II describes the noise received at the towed array and the dealiasing of the AC signal. Section III describes the signal processing associated with the autocorrelation functions of the signals, including the electrical feed-over, the undesirable time sidelobes caused by a spectral ripple, the whitening filter used to mitigate its effects, and the coherent stacking process to isolate the bottom echo. Section IV describes the measurement of the reflection loss. Section V shows the results of the reflection analysis, followed by the conclusions in Section VI.

## II. THE NOISE

The data collected were divided in time into four sections numbered 1 to 4. Each section corresponded approximately to one loop around the designated path. Each section was subdivided into two approximately equal parts: 1 and 2. The data in each part ranged between 200 and 350 s in duration. For autocorrelation and cross-correlation processing, the data in each part

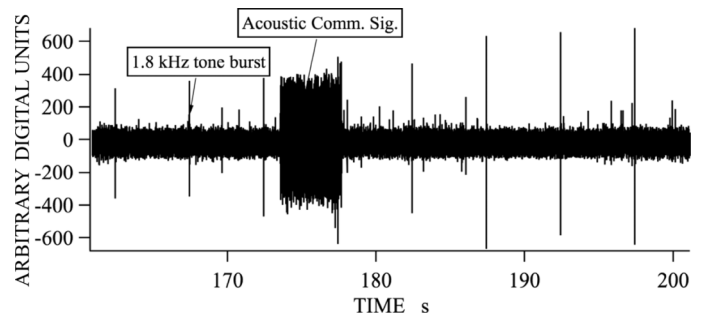


Fig. 2. An example of the time series signal at a receiver.

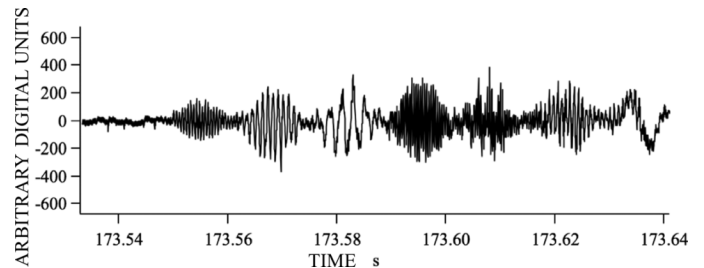


Fig. 3. An example of the AC burst, expanded to show the FSK data packets.

were subdivided into 40-s contiguous blocks. Given the signal bandwidth of approximately 10 kHz, a 40-s block could contain up to 400 000 independent samples, which should be adequate for constructing statistically meaningful correlation functions. An example of a block is shown in Fig. 2. It contains a noise floor, periodic tone bursts (TB) from an offboard source, and an AC signal packet, as illustrated in the figure. There was usually one AC burst in every 40-s block of data, indicating that the repetition period was approximately 40 s.

Since the sound source was essentially incoherent noise, there were no identifiable signal pulses. The autocorrelation and the cross correlation of the noise are fundamental. The noise floor in between the TB and AC bursts was tested for autocorrelation features. No features were found, therefore it must be concluded that the noise floor is not related to any self-noise generated by the AUV. The TB bursts were not used because they do not originate from the AUV, but from a distant offboard source. Therefore, all the processing was done with the AC bursts. The AC source was located on the underside of the AUV at approximately amidships, as shown in Fig. 1(a). The AC burst consisted of a series of tones, characteristic of frequency shift key (FSK) data transmission, as shown in the sample in Fig. 3.

Examples of the power spectrum at each receiver are shown in Fig. 4(a). The sampling rate was 20 756 samples/s, therefore the unambiguous spectrum extended up to a maximum frequency of 10378 Hz. The levels in receivers 3 and 8 were at least 10 dB below that of the other receivers. Apart from the differences in level, all the spectra appeared to be similar. The first 250 Hz, or so, appears to be contaminated with  $1/f$  noise. The AC signal spectrum, which apparently covers the band from zero to 4.5 kHz and is modulated at an approximate period of 300 Hz, is most prominent. This was determined to be an alias of the true AC signal, since it was known to be centered about 18 kHz. The dealiased spectrum was recovered as shown in

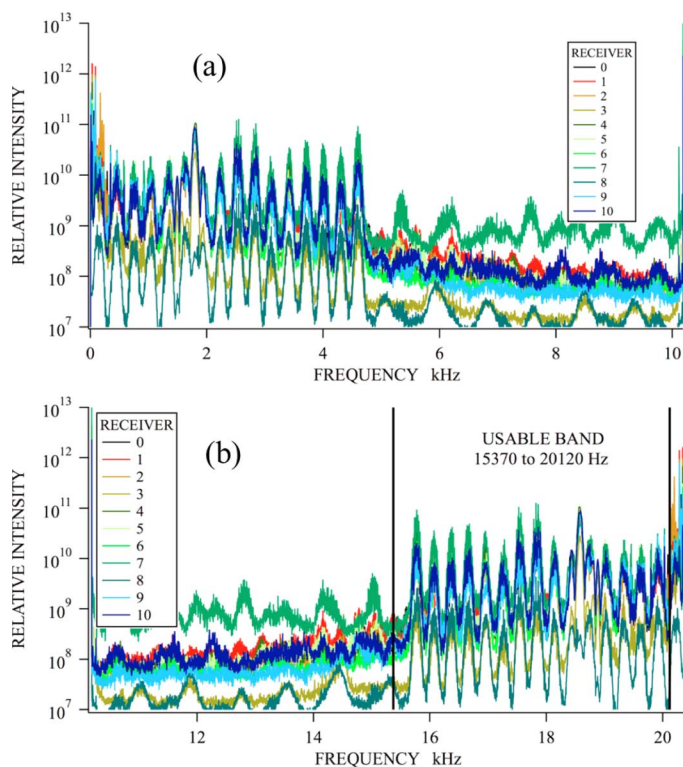


Fig. 4. (a) An examples of signal power spectrum at each receiver, showing a noise background and the aliased AC spectrum. (b) Dealiasied AC signal spectrum at each receiver, showing the usable band.

Fig. 4(b). The usable band extends from around 15 to 20.120 kHz. A margin of 250 Hz was left at the upper end to avoid the  $1/f$  noise that would have aliased into this part of the band. All subsequent processing was performed on the dealiasied signal and within the indicated usable band.

### III. AUTOCORRELATION

The AC signal was isolated in each data block and the autocorrelation  $C_i(t)$  of the dealiasied AC signals at the  $i$ th receiver was computed from the power spectrum. The autocorrelation functions were normalized to unity at  $t = 0$ . A typical set of normalized autocorrelation function amplitudes is shown in Fig. 5(a). This example was taken from one of the blocks of data after the AUV and towed array had settled into a stable configuration.

The autocorrelation functions of an acoustic signal, projected from the AUV and received on the towed array, were simulated using the model in Fig. 1(a). In accordance with the description of the experiment, the source and receiver depths  $d_s$  and  $d_i$  were set at 2 m. The nominal bottom depth  $d_b$  was 9.5 m. The horizontal distance  $x_o$  between the sound source and the closest receiver was set at 6 m. The receiver separation  $x_d$  was 0.75 m, as shown in Table I. For the sake of argument, the nominal bottom-reflection coefficient was set at  $-10.5$  dB, which would correspond to a sandy seabed. A simple ray model, which accounted for the spherical spreading loss and the reflection loss at each interface, was used to generate the impulse response of the sound path between the source and the receivers,

assuming flat surface and bottom interfaces. The impulse responses were bandpass filtered to match the band width of the AC burst, and used to generate the simulated autocorrelation functions as shown in Fig. 5(b). The simulation shows a ridge in the autocorrelations (DIR\_BOT) due to the cross correlation between the direct path signal and the bottom reflection, and a weaker ridge due to the surface-bottom-reflected multipath (DIR\_BOT,SURF). The path abbreviations are defined as they occur in the text, and, in addition, they are listed in Table II.

The surface-reflection ridge (DIR\_SURF) is difficult to identify in the simulation because the path difference between it and the direct path signal is too small. In the measured correlation functions, it may be absent because, due to the position of the source on the underside of the AUV, it is obstructed by the AUV itself. It is evident that, at this point, the measured and simulated autocorrelation functions look nothing alike. The DIR\_BOT ridge cannot be identified in the measured autocorrelations in Fig. 5. The ridges in the measured autocorrelations are slanted in the opposite direction than those in the simulation.

A number of hypotheses, both acoustical and mechanical, were considered, including deviations of the array from its nominal horizontal configuration, crosstalk between channels, and even the possibility that the direct path signal was distorted by the wake of the AUV. None of them could explain the differences, therefore we examined possible solutions to this inconsistency.

#### A. Electrical Feed-Over

The most probable cause of the discrepancy was neither acoustic nor mechanical, but electrical. There was significant electrical feed-over of the AC signal into the acoustic receivers. When the raw signals from all the receivers were compared, it was noticed that they appeared to have a common component. When they were coherently averaged, the result did not tend to zero, as shown in Fig. 6(a), and in greater detail in Fig. 6(b).

The average signal, since it is coherent across all the receiver channels, without any time displacement, must be indicative of an electrical feed-over. The simulation was modified to include a component of feed-over and the result, as shown in Fig. 7, contains a ridge due to the cross correlation between the feed-over and the direct path (FO\_DIR) that looks similar to the strongest ridge in the measured data in Fig. 5(a). The position of this ridge on the time axis is equal to the travel time from the source to the receivers.

From the measured data in Fig. 5(a), it was confirmed that the distance from the closest receiver to the sound source  $x_o$  was approximately 6 m, and the slope of the ridge confirms that the receiver separation  $x_d$  was 0.75 m, given a sound speed of 1530 m/s, which is typical for the summer months at this site. A ridge due to the cross correlation between feed-over and the bottom-reflected signal (FO\_BOT) is also expected, as shown in Fig. 7. Although the electrical feed-over was unexpected and unwanted, its presence is fortuitous because it provided a means of checking the distance between the source and the receivers.

#### B. Spectral Ripple

Another characteristic of the measured autocorrelation functions in Fig. 5(a) is the periodicity of the ridges, which was

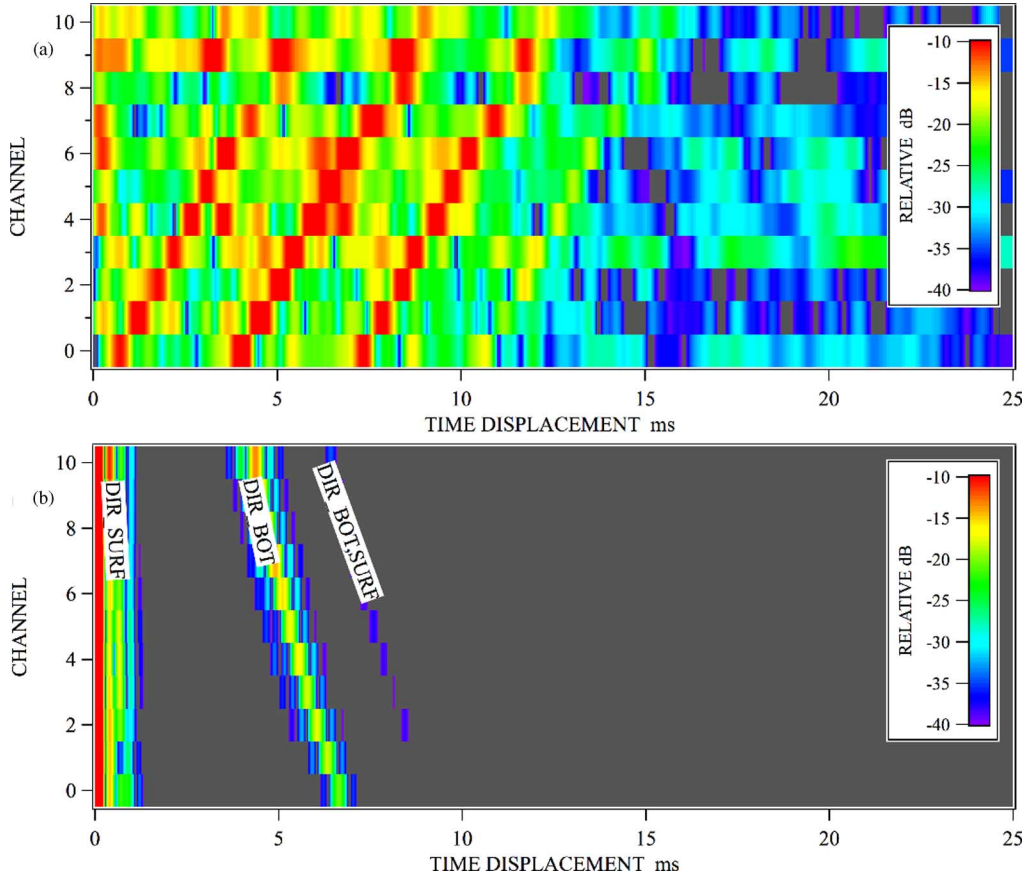


Fig. 5. (a) An example of measured autocorrelation functions of the dealiased AC signals at each receiver. (b) An example of simulated autocorrelation functions of the signals at each receiver, showing a ridge due to the direct path and bottom-reflection signals (DIR\_BOT) and another ridge due to the surface-bottom-reflected multipath (DIR\_BOT,SURF).

TABLE I  
NOMINAL DISTANCES

Symbol	Quantity	value - m
$d_b$	water depth	9.5
$d_s, d_i$	source, receiver depth	2
$x_o$	trail back	6
$x_t$	receiver separation	0.75

TABLE II  
ABBREVIATIONS

Abbreviation	Cross-correlation peak between	
$DIR\_BOT$	acoustic direct path	bottom reflected path
$DIR\_SURF$	acoustic direct path	surface reflected path
$DIR\_BOT,SURF$	acoustic direct path	surface and bottom reflected
$FO\_BOT$	electrical feed-over	bottom reflected path
$FO\_DIR$	electrical feed-over	acoustic direct path
$FO\_DIR+nREP$	electrical feed-over	nth ghost of acoust. direct path
$FO\_nREP$	electrical feed-over	nth ghost of elect. feed-over

traced to the ripples in the signal spectrum, an example of which is shown in Fig. 8(a). These ripples exist because the AC signal is an FSK communication signal with discrete frequency channels. Fourier's theorem tells us that periodic structures in the

frequency domain produce peaks in the time domain and *vice versa*.

This feature was added to the simulation by modulating the simulated signal spectrum with the square of a raised sine wave ripple of the same period, as shown in Fig. 8(b). The resulting simulated autocorrelation functions are shown in Fig. 9(b). There are now periodic vertical ridges due to repetitions, or ghosts, of the feed-over (FO\_REP), and repetitions of the slanted ridges due to the feed-over and direct path ridges (FO\_DIR+nREP). The simulation now has all of the main features of the measured autocorrelation functions. The periodically repeating features are clearly undesirable because they have a tendency to contaminate the correlation ridges that are sought, particularly the bottom-reflection-related features DIR\_BOT and FO\_BOT. It can be seen that DIR\_BOT would be very difficult to detect, but FO\_BOT may still be detectable.

### C. Spectral Whitening

To reduce the periodic repetitions in the measured autocorrelation functions, the spectrum of each channel was whitened by dividing by the measured root mean square (RMS) average spectrum from all the channels, and then windowed with a raised cosine taper to reduce the time sidelobes of the autocorrelation ridges. An example of the filter is shown in Fig. 8(c). This produced an improvement in the measured autocorrelation functions, as shown in Fig. 9(a).

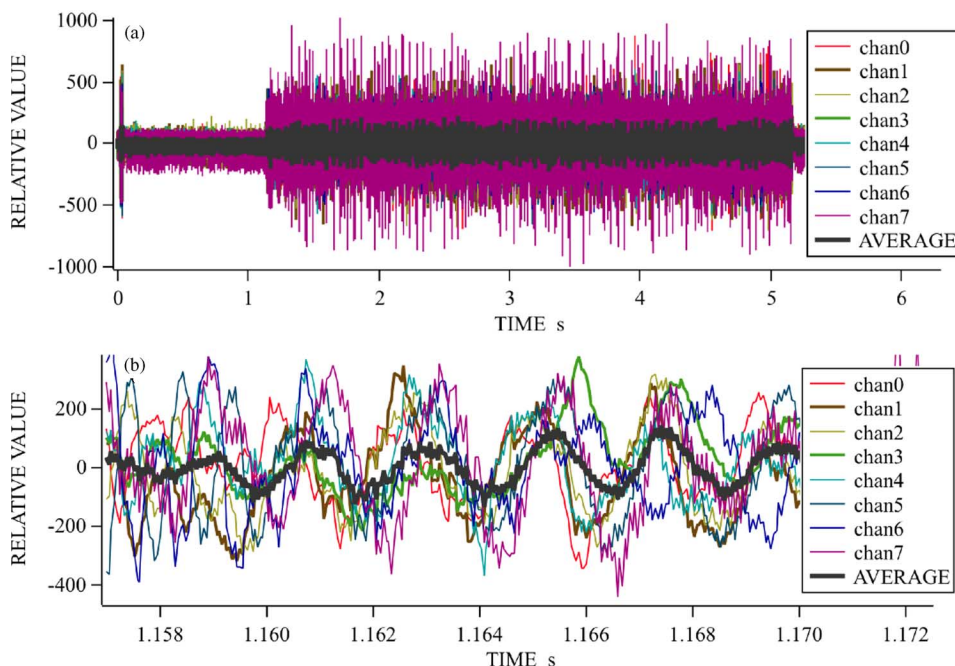


Fig. 6. (a) An example of the AC signal from channels 0 to 7, and their average. (b) A magnified section of the AC signal from channels 0 to 7, and their average, showing the coherence between each channel and the average.

The dominant correlation ridges, computed from the eigenrays and clearly seen in the simulation of Fig. 9(b), are superimposed on the measured autocorrelation functions in Fig. 9(a). These include the cross correlations of the direct path and surface-reflected signals (DIR\_SURF), the feed-over and direct path signals and its aliases (FO\_DIR+nREP), and the feed-over and bottom-reflected signal (FO\_BOT), in addition to the ones mentioned above. The cross correlation between the electrical feed-over and the direct path arrival (FO\_DIR) was the strongest feature, and it provided some additional information about the array configuration as stated previously.

Before going on, it should be noted that the signal at channel 8 appears irregular. It was later found to have functional problems. Its FO-DIR peak is out of sequence compared to the other channels. The peaks in channel 10, the last element at the end of the array, appear significantly weaker than those of the other channels, which suggests a degree of incoherence, possibly due to random motion relative to the other elements. Since there was no array stabilization device (such as a drogue) at the end of the array, it is possible that the last two elements had some undesirable motion. For these reasons, channels 8, 9, and 10 will not be used in the estimation of bottom reflection.

#### D. Stacking

Coherent stacking was used to pull the bottom-reflected correlation peak out from the interference. The complex autocorrelation functions from contiguous blocks were coherently stacked. An example is shown in Fig. 10. Typically, there were between four and six contiguous blocks in each section of data. The autocorrelations from all the receivers were coherently stacked according to the estimated arrival times for a range of water depths (9–12 m). It was necessary to limit the search to 9 m or greater, to avoid interference by the aliased FO\_DIR

ridges. The final coherent stack shows a peak at a position close to the nominal 9.5-m water depth of the experimental site, indicative of the presence of the FO\_BOT ridge, even though the ridge itself is difficult to see.

#### IV. ESTIMATION OF BOTTOM-REFLECTION LOSS

The reflection loss is a calibrated quantity. In the absence of calibration, the reflection coefficient magnitude  $|R_i(\theta)|$ , as a function of grazing angle  $\theta$ , may be defined in terms of the ratio between the direct path signal  $|S_{iD}|$  and the bottom-reflected signal  $|S_{iR}|$  amplitudes, at array element number  $i$ , after compensating for differences in spreading loss, absorption, and directivity functions

$$|R_i(\theta)| = \frac{|S_{iR}| |D_{iD}| r_{iR} \exp(\alpha r_{iR})}{|S_{iD}| |D_{iR}| r_{iD} \exp(\alpha r_{iD})} \quad (1)$$

where  $r_{iD}$  and  $r_{iR}$  are the path lengths, and  $D_{iD}$  and  $D_{iR}$  are directivity functions, from the source to the receiver along the direct and reflected paths, respectively, and  $\alpha$  is the absorption coefficient. It is assumed that the sound speed in the water may be approximated by a constant. This is a valid assumption, because the path lengths are very short, and because the sound-speed profile at the site was known to be benign. The absorption may be ignored because it is estimated to be less than 0.004 dB/m, and the path lengths are less than 20 m, giving absorption losses of less than 0.1 dB. The AC source directivity may be considered approximately uniform in the horizontal and downward directions. The directivity in the upward directions is likely obstructed by the AUV itself. The beam pattern of the source transducer is independent of the azimuth angle, and shows a smooth variation as a function of depression/elevation angle that decreases with decreasing frequency [10]. At 20 kHz, the variation was down to less than a 2-dB difference between the direct

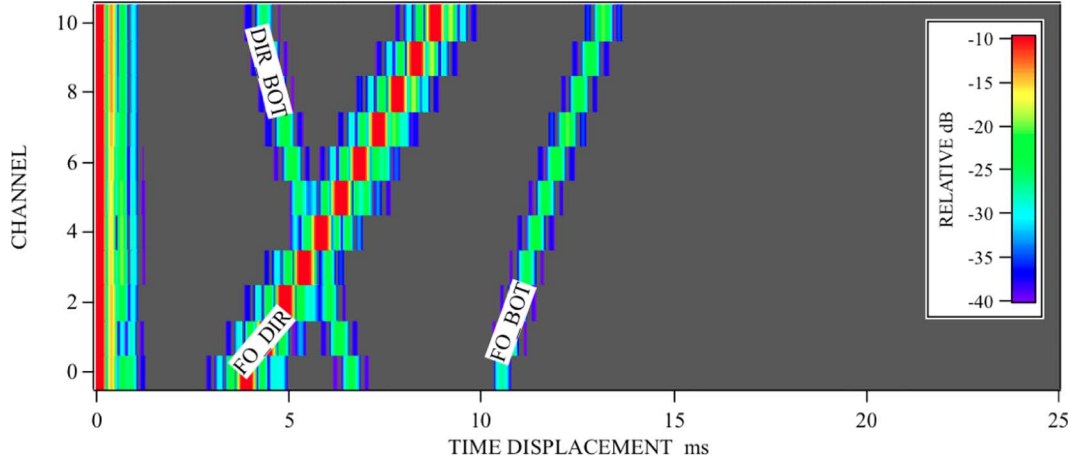


Fig. 7. Simulated autocorrelation functions with feed-over. The ridges due to the correlation between feed-over and direct path (FO\_DIR) and the bottom reflection (FO\_BOT) are shown along with the ridge DIR\_BOT from Fig. 5(b).

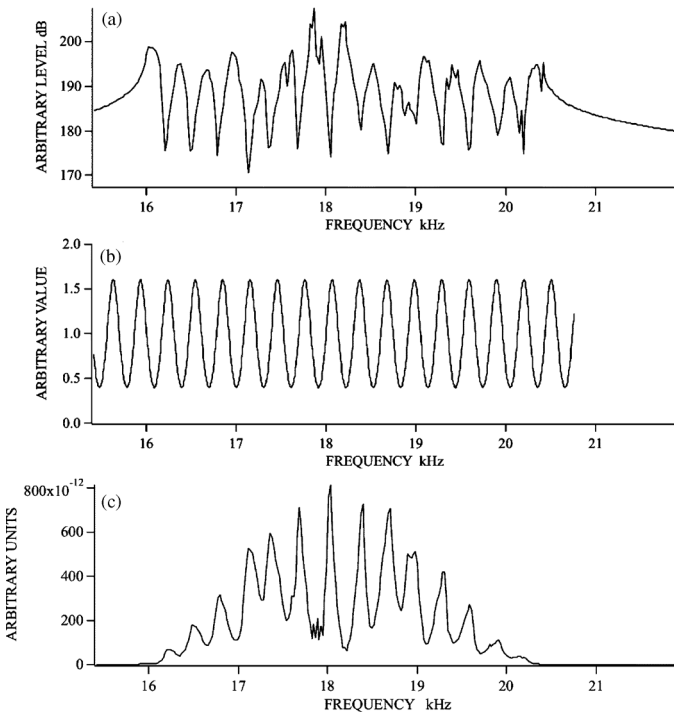


Fig. 8. (a) An example of the measured signal power spectrum showing strong ripples at a period of approximately 305 Hz in the frequency domain. (b) Spectral ripples modulated onto the simulated signals. (c) A whitening bandpass filter obtained by averaging the power spectra of all channels, combined with a raised cosine taper to reduce time sidelobes.

path direction (horizontal) and the bottom-reflected path direction ( $62^\circ$  down from the horizontal). However, the directivity function of the array elements, in the applicable frequency band, is far from uniform. Each array element consists of a small horizontal array of six serially connected sensors, with their centers spaced at 10.5 mm apart. The directivity function of the element, for the frequency band shown in Fig. 8(c), was computed, and it is shown in Fig. 11. This figure shows the effective directivity function for acoustic signals with the average spectral density shown in Fig. 8(c). A reduction of 10 dB in the horizontal (direct path) direction is predicted.

The ratio of the reflected to the direct path signal amplitudes may be obtained from the ratio of the autocorrelation amplitude at FO\_BOT to that at the FO\_DIR positions. The former is the cross correlation between the feed-over and the bottom-reflected signal, and the latter is the cross correlation between the feed-over and the direct path signal. One contains a product of the feed-over and bottom-reflected signal amplitudes, and the other contains the product of the feed-over and the direct path signal amplitudes. Dividing one by the other eliminates the feed-over amplitude, leaving the ratio of the reflected and direct path signal amplitudes

$$\frac{|S_{iR}|}{|S_{iD}|} = \frac{|C_i(t_{i,FO\_BOT})|}{|C_i(t_{i,FO\_DIR})|} \quad (2)$$

where  $t_{i,FO\_BOT}$  and  $t_{i,FO\_DIR}$  are the delay times of the respective correlation peaks, and  $|C_i(t)|$  is the amplitude of the autocorrelation function of the  $i$ th array element at time  $t$ , as illustrated in the example in Fig. 9(a). Thus, the method does not require any source or receiver calibration. An example of a similar self-calibrating method is given in [11]. The peak at  $t_{i,FO\_DIR}$  is very prominent and easily detected. The simulation in Fig. 9(b) suggests that the peak at  $t_{i,FO\_BOT}$  should also be clearly detectable, but that was because a reflection amplitude of  $-10.5$  dB was assumed in the simulation, which would be appropriate for a hard bottom such as sand. The peak at  $t_{i,FO\_BOT}$  in the measured correlation function, as shown in Fig. 9(a), is very weak and difficult to detect, suggesting a much softer bottom.

The coherent stack, as shown in Fig. 10, was used to estimate the position of the bottom-reflection peak FO\_BOT. However, the level of the stacked peak is not expected to be a good measure of the individual correlation peaks, because it is known from experience that bottom reflections contain a significant component of random spatial variability. At lower frequencies below approximately 10 kHz, mesoscale spatial variations  $O(1 \text{ to } 10^3)$  m as mentioned in [6] will have a significant effect. At higher frequencies, the causes of variability

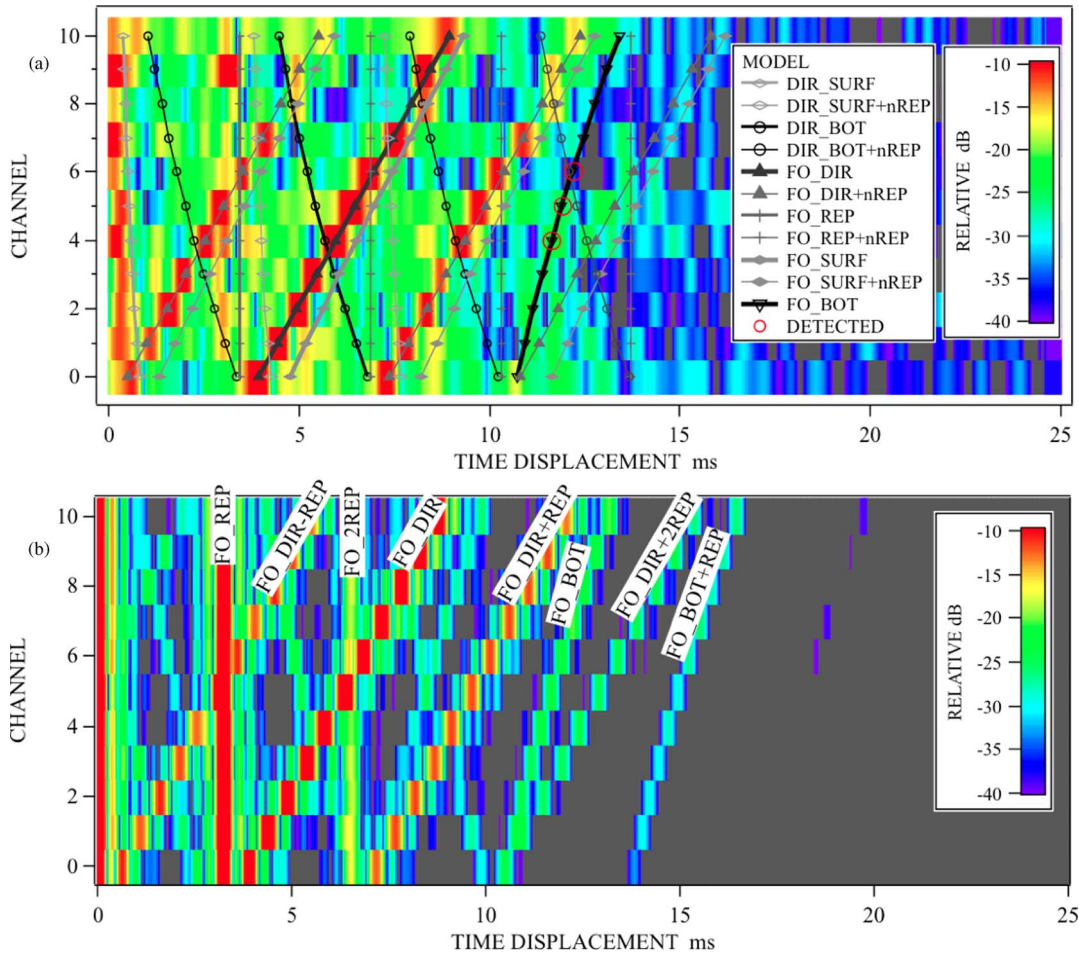


Fig. 9. (a) An example of the measured autocorrelation functions, and the expected ridges. (b) An example of simulated autocorrelation functions with feed-over and spectral ripples, showing periodically repeating ridges FO\_REP, FO\_DIR-, and FO\_DIR+REP.

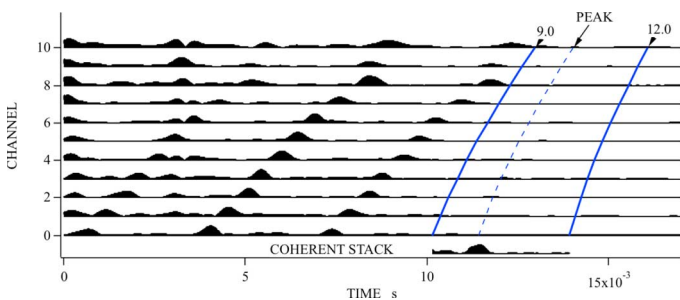


Fig. 10. An example of the normalized squared magnitudes of coherently stacked complex autocorrelation functions from five contiguous blocks, and the normalized result of coherently stacking all receivers to find the bottom-reflection peak.

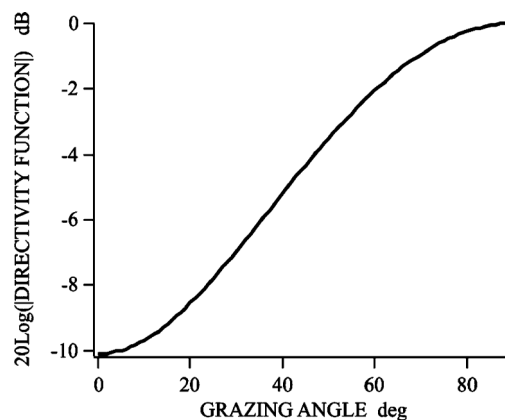


Fig. 11. Directivity function of the receiver elements.

include smaller scale variations  $O(10^{-3} \text{ to } 1) \text{ m}$ , such as interface roughness and volume inhomogeneities [12], variations in the bulk sediment properties, and bottom dwelling biological organisms [13]. The result is a random component in the bottom-reflection coefficient that changes as a function of position over a range of scales. Since the signal at each receiver is reflected from a different patch of the bottom, they also contain a random component that differs from one receiver to another. The random component would have been greatly reduced by the coherent stacking process. Therefore, the loca-

tion of the peak from the coherent stack was used to construct a window within which to look for the peak in each individual autocorrelation function. If a peak was detected within  $\pm 0.25 \text{ ms}$  of the estimated location, then its value was accepted. Otherwise, it was rejected.

With reference to the ray diagram in Fig. 1(a), the grazing angle  $\theta$ , i.e., the angle between the incident ray and the horizontal seabed, may be related to the travel time difference

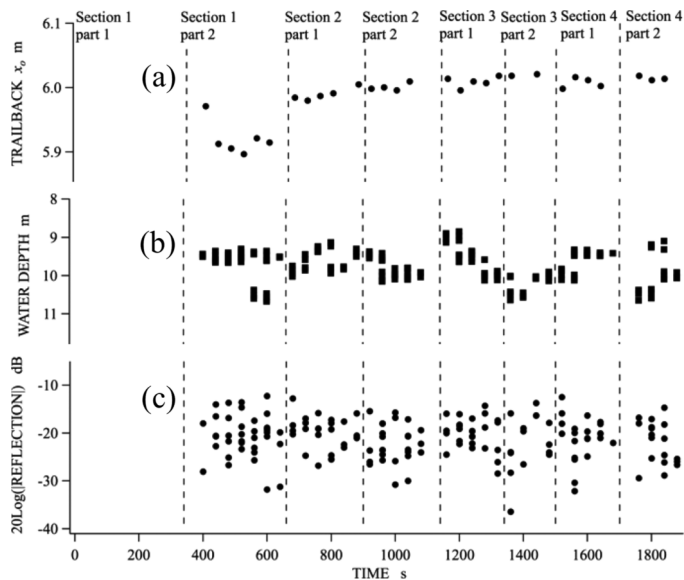


Fig. 12. (a) Measured trail-back distance, from the source to the nearest receiver, as a function of time in each data block. (b) Water depth estimates from the detected FO\_BOT peaks. (c) Measured bottom-reflection loss; the average grazing angle was  $62^\circ$ . The dotted lines mark the boundaries between data sections.

$(t_{i,FO\_BOT} - t_{i,FO\_DIR})$ , the speed of sound,  $c$ , and the height above the seabed ( $d_b - d_s$ ) by

$$\tan(\theta) = \frac{2(d_b - d_s)}{(t_{i,FO\_BOT} - t_{i,FO\_DIR})c}. \quad (3)$$

## V. RESULTS

The FO\_DIR ridge was used to estimate the distance from the source to the nearest receiver. The position of the FO\_DIR peak is the travel time from the source to each receiver. Multiplying the travel time by the speed of sound gives the distance. This distance is called the trail back. The results are shown in Fig. 12(a). The autocorrelation functions in the first section of data did not show an identifiable FO-DIR ridge, most likely because the towed array was not yet in a stable configuration. The results in the second section show some variation in the trail back, indicating that the array was settling down. Subsequent sections show a stable trail back, indicating that the array had reached a stable configuration. From the detected FO\_BOT peaks, water depth estimates were made as shown in Fig. 12(b). These were obtained from the detected peaks of the individual autocorrelation functions, within the window computed from the coherently stacked peak. They show variations about the nominal 9.5-m depth for the test site.

Using the measured auto-correlation peaks at FO\_DIR and FO\_BOT, the seabed-reflection loss and grazing angle were estimated using (1) and (2). There were a total of 170 detected FO\_BOT peaks from which reflection loss calculations were made. The reflection loss values are shown in Fig. 12(c). It shows variations about a mean value of  $-21$  dB, and a standard deviation of 4.9 dB. The latter is consistent with standard deviations observed at similar frequencies and ranges in a previous experiment [12]. The grazing angle was estimated using

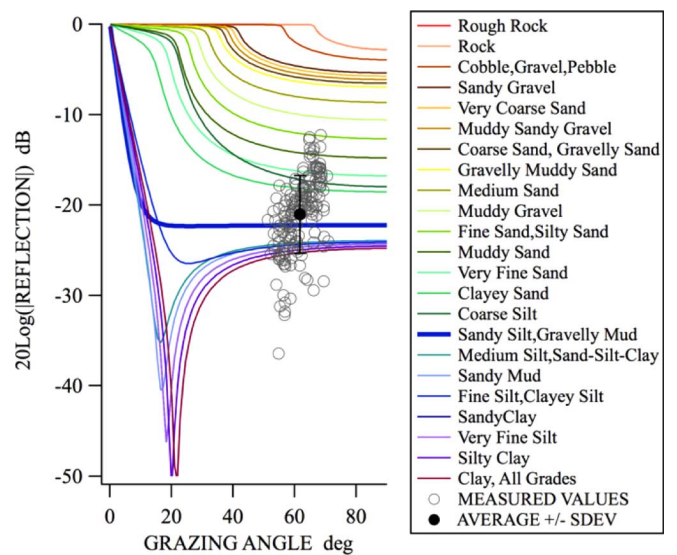


Fig. 13. Reflection loss as a function of grazing angle compared to the HFEVA model curves.

(3) and its average value was  $62^\circ$ , with a standard deviation of  $5^\circ$ .

A sediment classification may be obtained by comparing the measured reflection losses and grazing angles with the high-frequency environmental acoustic (HFEVA) seabed model [14], which is claimed to be valid between 10 and 100 kHz. A scatter plot of the measured reflection loss values, as a function of grazing angle, is shown in Fig. 13. Due to the geometry of the towed array system and the distances to the boundaries, only angles between  $50^\circ$  and  $70^\circ$  were realized. Comparing the measured values with the model curves, it would appear that the measured reflection values fall between “muddy sand” and “clay, all grades.” The average reflection loss was 21 dB, which is closest to the “sandy silt, gravelly mud” curve. This is qualitatively consistent with what is known about the test site. A detailed survey of the Gulf of La Spezia states that “the sea floor of the inner gulf consists entirely of grey clay with virtually no bottom relief” [15].

## VI. CONCLUSION

It was demonstrated that the self-noise of an AUV, in conjunction with a towed line array, may be used to measure the bottom-reflection loss and obtain an estimate of the seabed type. In this case, the self-noise was the AC signal. There were a few complications, which made the project challenging and unique. 1) There were no recordings of the transmitted AC signal. Therefore, it had to be treated as a random noise and only its statistical properties, particularly the autocorrelation and cross-correlation functions, could be relied upon. 2) There was a strong electrical feed-over from the AC projector into the receiving amplifiers, but instead of being a hindrance, it was useful for estimating the separation between the source and the receivers. 3) The autocorrelation function of the AC signal had undesirable time side-lobes, which limited the sample space of the seabed-reflection signal. 4) The sediment at the test site was very soft, and, consequently, the reflected signal was weak, and it was necessary to coherently stack the correlation functions to find the seabed

echo. The approach adopted was to separate the direct path and the bottom-reflected signals. The amplitude ratio of the bottom reflected to the direct path signal levels, after compensating for the differences in absorption, spreading losses, and beam patterns, yields the seabed-reflection loss, at the applicable grazing angle. The latter is calculated from the travel time difference between the direct and bottom-reflected signals and the known source–receiver separation. The method is self-calibrating and requires absolute calibration of neither the sound source nor receivers. The definitive isolation of the reflected and direct path signals and the self-calibrating property make this approach robust. The measured reflection loss at the experimental site had an average of 21 dB with a standard deviation of 4.9 dB, at a mean grazing angle of 62°. Comparing the measurements with the HFEVA model, the sediment type was estimated to be closest to “sandy silt, gravelly mud.”

#### ACKNOWLEDGMENT

The authors would like to thank their colleagues, particularly M. Chitre and M. Isakson, for many useful discussions, and they acknowledge the NURC for the support in providing the OEX platform for the data collection.

#### REFERENCES

- [1] N. H. Gholson and M. G. Fagot, “A deep-towed sound source and hydrophone array system-performance analysis and design,” in *Handbook of Geophysical Exploration at Sea*, R. A. Geyer, Ed. Boca Raton, FL: CRC Press, 1983, pp. 35–86.
- [2] J. F. Gettrust, J. H. Ross, and M. M. Rowe, “Development of a low frequency, deep tow geoacoustic system,” *Sea Technol.*, vol. 32, pp. 23–32, Sep. 1991.
- [3] C. W. Holland and J. Osler, “High-resolution geoacoustic inversion in shallow water: A joint time- and frequency-domain technique,” *J. Acoust. Soc. Amer.*, vol. 107, no. 3, pp. 1263–1280, 2000.
- [4] J. D. Holmes, W. M. Carey, and J. F. Lynch, “Results from an autonomous underwater vehicle towed hydrophone array experiment in Nantucket Sound,” *J. Acoust. Soc. Amer.*, vol. EL 120, pp. EL15–EL21, 2006.
- [5] A. Maguer, R. Dymond, P. Guerrini, L. Troiano, V. Grandi, A. Figoli, C. Olivero, A. Sapienza, S. Fioravanti, and J. Potter, “Receiving and transmitting acoustic systems for AUV/gliders,” in *Proc. 3rd Int. Conf. Underwater Acoust. Meas., Technol. Results*, Nafplion, Greece, 2009, paper 32–4.
- [6] C. W. Holland, P. L. Nielsen, J. Dettmer, and S. E. Dosso, “Resolving meso-scale seabed variability using reflection measurements from an autonomous underwater vehicle,” *J. Acoust. Soc. Amer.*, vol. 131, pp. 1066–1078, 2012.
- [7] D. J. Battle, P. Gerstoft, W. A. Kuperman, W. S. Hodgkiss, and M. Siderius, “Geoacoustic inversion of tow-ship noise via near-field-matched-field processing,” *IEEE J. Ocean. Eng.*, vol. 28, no. 3, pp. 454–467, Oct. 2003.
- [8] V. Pallayil, M. A. Chitre, and P. D. Deshpande, “A digital thin line towed array for small autonomous underwater platforms,” in *Proc. MTS/IEEE OCEANS Conf. Exhibit.*, Vancouver, BC, Canada, Sep.–Oct. 29–4, 2007, DOI: 10.1109/OCEANS.2007.4449123.
- [9] V. Pallayil, S. S. Muttuthupara, M. A. Chitre, K. Govind, V. and N. R. Chandhavarkar, “Characterisation of a digital thin line towed array – Experimental assessment of vibration levels and tow shape,” in *Proc. 3rd Int. Conf. Underwater Acoust. Meas., Technol. Results*, Nafplion, Greece, Jun. 21–26, 2009, paper 32–2.

- [10] BTech Acoustics LLC, “Specifications of model BT-2RCL transducer,” 2010 [Online]. Available: <http://acomms.whoi.edu/documents/211002-SPC%20WH-BT-2%20Datasheet.pdf>
- [11] N. P. Chotiros, A. P. Lyons, J. Osler, and N. G. Pace, “Normal incidence reflection loss from a sandy sediment,” *J. Acoust. Soc. Amer.*, vol. 112, pp. 1831–41, 2002.
- [12] N. P. Chotiros, M. J. Isakson, J. N. Piper, and M. Zampolli, “Modeling of reflection coefficient fluctuation from measured seafloor roughness,” in *Proc. MTS/IEEE OCEANS Conf. Exhibit.*, Vancouver, BC, Canada, Sep.–Oct. 29–4, 2007, DOI: 10.1109/OCEANS.2007.4449151.
- [13] N. P. Chotiros and T. H. DeWitt, “Acoustic sediment properties and the abundance of burrowing shrimp in marine sediments from reflection measurements,” in *Proc. 5th Eur. Conf. Underwater Acoust.*, Villeurbanne, France, Jul. 10–13, 2000, pp. 781–786.
- [14] “APL-UW high-frequency ocean environmental acoustic models handbook,” Appl. Phys. Lab., Univ. Washington, Seattle, WA, APL-UW 9407, 1994.
- [15] L. R. Breslau and H. E. Edgerton, “The sub-bottom structure of the Gulf of La Spezia,” SACLANT ASW Res. Centre, La Spezia, Italy, Tech. Rep. 129, 1968.



**Nicholas P. Chotiros** (M’89) received the B.A. degree in engineering from Cambridge University, Cambridge, U.K., in 1973 and the Ph.D. degree in electronic and electrical engineering from University of Birmingham, Birmingham, U.K., in 1981, specializing in underwater acoustics.

From 1974 to 1982, he worked on a number of projects in underwater acoustics at the University of Birmingham, as a Research Associate and as a Lecturer. Since 1982, he has been with the Applied Research Laboratories, The University of Texas at

Austin, Austin, currently as a Research Scientist, and worked on a number of projects in underwater acoustics. He served as a Program Officer at the Office of Naval Research between 2002 and 2005. Currently, he specializes in ocean sediment acoustics, including reflection, transmission, and scattering.

Dr. Chotiros is a Fellow of the Acoustical Society of America (ASA). He serves the local chapter of the IEEE as a liaison for the student branch of the University of Texas at Austin. He is an Associate Editor of the *Journal of the Acoustical Society of America* and of the *IEEE JOURNAL OF OCEANIC ENGINEERING*.



**Venugopalan Pallayil** (SM’04) received the M.Sc. degree in physics and the Ph.D. degree in microwave electronics from Cochin University of Science and Technology, Kerala, India, in 1981 and 1992, respectively.

From 1986 to 1998, he served as an R&D Scientist in the Defence Research and Development Organisation, India, contributing to the development of airborne ASW sensors. In late 1998, he joined the Acoustic Research Laboratory (ARL), Tropical Marine Science Institute (TMSI), National University of Singapore, Singapore, as a Research Fellow. Currently he is a Senior Research Fellow and Deputy Head at ARL and also supports TMSI as Operations Manager. At ARL, he has been actively involved and led many projects including underwater ambient noise imaging, time reversal mirror experiments, and digital thin line array development. He has a strong interest in the development of AUV-based sensors and applications.

Dr. Pallayil was one of the leading members of the team which won the Defence Technology Prize 2004 for the project ROMANIS on ambient noise imaging. As an active IEEE member, he has served the local OES Chapter in many capacities, including the Chairmanship, and was also the Chair for Finance for the Oceans2006 Conference in Singapore. He is also a member of Acoustical Society of America.